Sciencexpress Report

A Persistent Oxygen Anomaly Reveals the Fate of Spilled Methane in the Deep Gulf of Mexico

John D. Kessler,[1]* David L. Valentine,[2]* Molly C. Redmond,[2] Mengran Du,[1] Eric W. Chan,[1] Stephanie D. Mendes,[2] Erik W. Quiroz,[3] Christie J. Villanueva,[2] Stephani S. Shusta,[2] Lindsay M. Werra,[2] Shari A. Yvon-Lewis,[1] Thomas C. Weber[4]

[1]Department of Oceanography, Texas A&M University, College Station, TX 77843–3146, USA. [2]Department of Earth Science and Marine Science Institute, University of California, Santa Barbara, CA 93106, USA. [3]Geochemical and Environmental Research Group, Texas A&M University, College Station, TX 77843, USA. [4]Center for Coastal and Ocean Mapping, University of New Hampshire, Durham, NH 03824, USA.

*To whom correspondence should be addressed. E-mail: jkessler@ocean.tamu.edu (J.D.K.); valentine@geol.ucsb.edu (D.L.V.)

Methane was the most abundant hydrocarbon released during the 2010 Deepwater Horizon oil spill in the Gulf of Mexico. Beyond relevancy to this anthropogenic event, this methane release simulates a rapid and relatively short-term natural release from hydrates into deepwater. Based on methane and oxygen distributions measured at 207 stations throughout the affected region, we find that within ~120 days from the onset of release ~3.0×10^{10} to 3.9×10^{10} moles of oxygen were respired, primarily by methanotrophs, and left behind a residual microbial community containing methanotrophic bacteria. We suggest that a vigorous deepwater bacterial bloom respired nearly all the released methane within this time, and that by analogy, large scale releases of methane from hydrate in the deep ocean are likely to be met by a similarly rapid methanotrophic response.

The immense accumulation of methane (CH_4) in the marine sub seafloor is among the largest global carbon reservoirs (*1*) and has been implicated as a factor in past oceanic and climate change. Oceanic CH_4 released naturally through hydrocarbon seeps, hydrothermal vents, or decomposing clathrate hydrates or anthropogenically through oil and gas exploration has the potential to influence climate being a moderate absorber of infrared radiation (*2*) and ocean chemistry when it is oxidized either aerobically or anaerobically (*3*–*6*). Oceanic CH_4 has been implicated in ancient climate change (e.g. (*7*)) however little is known about potential future impacts (*8*). Importantly, for oceanic CH_4 to directly impact climate, CH_4 must enter the atmosphere without first being consumed by microbes in the ocean.

On April 20, 2010 a violent and tragic CH_4 discharge severed the Deepwater Horizon rig from its well. Two days later, the burning rig sank and oil and gas began spewing into the deep Gulf of Mexico at depths of ca. 1.5 km until July 15 when the well was effectively sealed. Estimates of the oil emitted during the 83-days of this disaster range from 4.1 to $4.4 \times 10^6 \pm 20\%$ bbls (*9*, *10*). The corresponding emission of methane (CH_4) could be as great as 1.25×10^{10} moles (*11*) or as low as 9.14×10^9 moles (Table 1) (*12*, *13*) depending on uncertainties in the gas to oil ratio and net oil emission. This localized CH_4 emission is of similar magnitude to the natural release rate of CH_4 to the entire Black Sea (*14*), and provided a unique opportunity to investigate the fate of CH_4 released into the deep ocean and to understand the response of cold-adapted methanotrophic bacteria.

The sea-air CH_4 flux measured during active flow (survey area approximately 25 km in diameter centered on the wellhead) indicates that even at elevated wind speeds, less than 6.8×10^5 moles (i.e. <0.01%) of the emitted CH_4 escaped to the atmosphere (*15*). The depth distributions of CH_4 in the vicinity of the wellhead measured during conditions of active flow displayed high CH_4 concentrations between 800-1200 m depth (*11*, *16*). This spatially consistent CH_4 distribution suggests that CH_4 remained dissolved and suspended in the deep waters between 800-1200 m depth as lateral intrusions from the main vertical release from the wellhead (*11*, *16*). These subsurface intrusion layers form as a result of trapping by density stratification of seawater entrained into the jet of oil/gas initially released from the wellhead as described previously (*17*); the empirical relationships derived from these previous experiments are consistent with intrusions at these depths for the scales of the Deepwater Horizon event (*17*). Hydrocarbon gases dissolved in the water column adjacent to the wellhead during active flow were present at relative proportions of 87.5%, 8.1%, and 4.4%, for CH_4, ethane (C_2H_6), and propane (C_3H_8), respectively, and the variations in their proportions and isotopic compositions suggested rapid respiration of C_2H_6 and C_3H_8 but not CH_4 (*11*).

To track the fate of CH_4, we conducted three expeditions to the oil spill site aboard the NOAA Ship *Pisces* after flow had ceased: 18 August – 2 September, 7 – 17 September, and

22 September – 4 October 2010. During these expeditions we tracked submerged hydrocarbon intrusions southwestward from the wellhead for 500 km using their concurrent fluorescence and oxygen anomalies (Fig. 1). We also quantified depth distributions of dissolved CH_4 and oxygen (DO) at 207 unique stations (110 for CH_4 and 202 for DO), using shipboard chemical techniques, and further analyzed CH_4 oxidation rates and the microbial community structure at seven representative locations (*13*).

Based on elevated CH_4 concentrations and pseudo-first order CH_4 oxidation rate constants of 0.001 day^{-1} (range: 0 – 0.013 day^{-1}, n = 22 minus one outlier) measured around the wellhead in June (*11*), as well as the generally low oxidation rates for CH_4 in deep waters along the continental margins (*6*), we expected CH_4 intrusions from the Deepwater Horizon to persist for years. However, our broad August – October surveys identified no instances of elevated CH_4 (Fig. 1). In fact, CH_4 concentration measurements conducted during all three expeditions yield an average CH_4 concentration of 1.43 ± 2.00 nM (max = 20.40 nM; n = 671), with the maximum concentration measured (20.4 nM) not exceeding ambient levels for the Gulf of Mexico (*18*). It is unlikely that CH_4 intrusions were simply missed during the survey, as concurrent fluorescence and DO anomalies were identified at most stations in the deep waters (Fig. 1C), indicative of both the presence of residual oil hydrocarbons and hydrocarbon respiration. Based on these results we hypothesize that methanotrophic bacteria consumed all CH_4 from the Deepwater Horizon event by the 18 August – 2 September survey.

As a first test of our hypothesis we integrated the DO anomaly for our study area (Fig. 1) and compared it to the potential oxygen demand exerted by the respiration of hydrocarbons released from the wellhead (Table 1). To calculate the oxygen anomaly for the entire intrusion, oxygen deficits were vertically integrated between 700-1300 m water depth for each station, and these integrated DO anomalies were contoured over the spatial extent of the intrusion (*13*). Bounds for the contouring on the northern and eastern edges were chosen based on bathymetric restrictions. On the southern and western edges, bounds were defined to encompass the DO and fluorescence anomalies measured with an average buffer of 50 km to incorporate any anomalies that may have been missed during sampling (Fig. 1A). The southern and western edges of the contour area were subsequently extended outward by 50 km to test the sensitivity of the calculation to changes in intrusion area (Fig. 1A). Five different contouring methods were used to constrain the sensitivity of the total DO removal estimates to the applied algorithm (Table S1) (*13*). The data collected during the first expedition (128 stations) were contoured separately from the second expedition (56 stations) to assess temporal variability; because the data collected during the third expedition (18 stations) did not adequately define the intrusion layer, an additional set of contour results were determined from a combined data set from expeditions 2 and 3. The integrated DO anomaly determined for the first expedition ranged from 3.00-3.90×10^{10} moles of O_2 removed, compared to 1.72-3.24×10^{10} moles of O_2 removed for the second and third expeditions. Mass balance dictates that respiration of CH_4 contributed substantially to the anomaly, and its magnitude is consistent with complete consumption of CH_4 and natural gas, along with partial respiration of oil (Tables 1 and S1).

As a second test of our hypothesis we cloned and sequenced 492 bacterial 16S rRNA genes from seven locations sampled during September 2010, searching for methylotrophic bacteria. Of these locations, four displayed DO and fluorescence anomalies at depth, whereas three did not. Despite the lack of CH_4, methylotrophic bacteria were detected at each site, with relative abundances ranging between 5-36% of sequences (Fig. 2 and S5). The microbial community in September 2010 differed significantly from the community identified around the wellhead in June, when no methylotrophs were detected and members of the *Oceanospirillales*, *Cycloclasticus* and *Colwellia* accounted for up to 100% of sequences (*11*, *19*). These groups are presumably involved in hydrocarbon oxidation, but have not been linked to methane oxidation. In September 2010, *Cycloclasticus* accounted for only 0-6% of sequences from each site, *Colwellia* for 0-5%, and the previously identified *Oceanospirillales* were not detected at all, though other members of this order accounted for 3-11% of sequences. This dramatic change in community composition is particularly striking considering that in September 2010 both methane concentrations (1.43 ± 2.00 nM; max = 20.40 nM; n = 671) and methane oxidation rates (avg = 0.0015 day^{-1}; range = 0.0006 – 0.0038 day^{-1}; n = 10) were very low, suggesting that methanotrophs were no longer active, and that we only observed the remnants of that population. Due to the lack of information on microbial communities present in the deep water column of the Gulf of Mexico before the Deepwater Horizon spill, it is difficult to determine background abundance of methylotrophs. However, even in areas of active methane seepage such as the Eel River and Santa Monica Basins, methylotrophs are present at such low relative abundances as to be virtually undetectable in 16S rRNA clone libraries (*20*). We were also able to sequence the particulate methane monooxygenase gene (pmoA) in select samples; these sequences were closely related to pmoA sequences from marine hydrocarbon seep environments (fig. S6). The unusually high relative abundances of methylotrophs observed in September, despite the fact that methylotrophs had likely decreased from their peak levels, strongly supports

our hypothesis that microbial methane oxidation was responsible for the disappearance of methane.

Taken together, the tracking of a hydrocarbon intrusion layer throughout the northern Gulf of Mexico, the paucity of CH_4 in the affected waters a month or more after the hydrocarbon emissions had ceased, the magnitude of the DO anomaly relative to emitted hydrocarbons (Table 1), and the prevalence of a methylotrophic microbial community (Fig. 2) suggest that CH_4 emitted from the Deepwater Horizon event was quantitatively consumed by August 2010. Given the slow rates of methanotrophy observed near the wellhead in June 2010 (*11*) we suggest a bloom of methanotrophic bacteria occurred in these waters sometime between the end of June and the beginning of August 2010, and that it likely occurred after affected waters had flowed away from the wellhead. This assertion is supported by previous observations that rates of methanotrophy increased as C_2H_6 was depleted in the hydrocarbon intrusions (*11*).

In order to better define the time-series change in CH_4 oxidation rates as well as CH_4 and DO loss, we created a one-dimensional time-dependent mixing, transport, and reaction model. The model fitted the measured CH_4 and DO concentration, and CH_4 oxidation rate data from the three expeditions as well as previous data collected in June (*11*) to interpolate the time course changes. The model predicts average DO anomalies in the intrusion layer of 38 μM by mid-September, which is greater than the average measured values of 5.6 ± 5.8 μM (n = 202), but in line with the largest DO anomalies (36.7 μM) measured in the 18 August – 2 September expedition. The model clearly overestimates the average DO anomaly especially because it only considers CH_4 oxidation when calculating the DO loss, ignoring the influence of C_2H_6, C_3H_8, and oil respiration. Since the total quantity of oxygen removed from the intrusion waters can only be explained by the complete oxidation of CH_4, C_2H_6, and C_3H_8 as well as the partial oxidation of oil, establishing a near complete mass balance (Table 1), the most logical explanation for the discrepancy between the modeled and measured average DO anomaly in September is that the model underestimates mixing. The model further predicts CH_4 oxidation rate constants increasing at the end of June and peaking at 0.2 day^{-1} at the end of July, followed by a return to the average measured values of 0.0015 day^{-1} (range = 0.0006 – 0.0038, n = 10) by mid-September (*13*) (Fig. 3). By using the rate constants as a proxy for population size we estimate a net doubling time of ~3.5 days for the methanotrophic bacteria assuming exponential growth at the peak rate constant of 0.2 day^{-1}. This is likely an upper limit as predatory effects are not considered. The specific CH_4 oxidation rates needed to explain complete consumption of intruded CH_4 are higher than for other deep pelagic environments (*6*, *21*) and indicate that there is no apparent limitation to the methanotrophic response to a CH_4 intrusion of this magnitude.

The oxidative lifetime of the deep CH_4 intrusion from Deepwater Horizon is approximately 120 days, with no measurable CH_4 loss to the atmosphere. The delay in methanotrophy compared to respiration of C_2H_6 and C_3H_8 (*11*) may be attributed to the difference in initial cellular abundance and growth rates of the responsible bacteria. However, methanotrophy proceeded more rapidly than dilution once the population became established and seemingly included exponential growth, limited ultimately by substrate availability.

Previous arguments have been forwarded for the massive release of CH_4 from the marine sub-seafloor in the geologic past (e.g. (*22*, *23*)). An open issue is the fate of released CH_4 and whether it enters the atmosphere, is oxidized in the ocean, or some combination of both processes (*24*, *25*). Our work suggests by analogy that large-scale CH_4 release to the deep ocean from gas hydrates or other natural sources may foster a rapid methanotrophic response leading to complete oxidation of CH_4 to CO_2 within a matter of months. Thus, aerobic methanotrophic bacterial communities may act as a dynamic biofilter that responds rapidly to large-scale CH_4 inputs into the deep ocean.

References and Notes

1. W. S. Reeburgh, in *Treatise on Geochemistry,* H. D. Holland, K. K. Turekian, Eds. (Elsevier - Pergamon, Oxford, 2003), vol. 4, pp. 65-89.
2. L. S. Rothman *et al.*, *Journal of Quantitative Spectroscopy & Radiative Transfer* **96**, 139 (Dec 1, 2005).
3. B. B. Ward, K. A. Kilpatrick, P. C. Novelli, M. I. Scranton, *Nature* **327**, 226 (1987).
4. M. J. Alperin, W. S. Reeburgh, M. J. Whiticar, *Global Biogeochemical Cycles* **2**, 279 (September, 1988).
5. W. S. Reeburgh *et al.*, *Deep-Sea Research* **38**, S1189 (1991).
6. D. L. Valentine, D. C. Blanton, W. S. Reeburgh, M. Kastner, *Geochimica et Cosmochimica Acta* **65**, 2633 (2001).
7. G. R. Dickens, in *Natural Gas Hydrates: Occurrence, Distribution, and Detection,* C. K. Paull, W. P. Dillon, Eds. (American Geophysical Union, Washington, DC, 2001), pp. 19-38.
8. A. G. Judd, M. Hovland, L. I. Dimitrov, S. G. Gil, V. Jukes, *Geofluids* **2**, 109 (2002).
9. T. J. Crone, M. Tolstoy, *Science* (2010) (10.1126/science.1195840).
10. USGS, "Deepwater Horizon MC252 gulf Incident Oil Budget: Government Estimates - Through August 01 (Day 104)" (2010). Available at: http://www.noaanews.noaa.gov/stories2010/PDFs/DeepwaterHorizonOilBudget20100801.pdf

11. D. L. Valentine *et al.*, *Science* **330**, 208 (2010).
12. Department of Energy. Deepwater Horizon Response. http://www.energy.gov/open/oilspilldata.htm
13. Materials and methods are available on *Science* Online.
14. J. D. Kessler *et al.*, *Earth and Planetary Science Letters* **243**, 366 (2006).
15. S. A. Yvon-Lewis, L. Hu, J. D. Kessler, *Geophysical Research Letters*, (2010) (10.1029/2010GL045928).
16. R. Camilli *et al.*, *Science* **330**, 201 (2010).
17. S. A. Socolofsky, E. E. Adams, *Journal of Hydraulic Engineering-Asce* **131**, 273 (2005).
18. J. M. Brooks, thesis, Texas A&M University (1975).
19. T. C. Hazen *et al.*, *Science* **330**, 204 (2010).
20. P. L. Tavormina, W. Ussler, V. J. Orphan, *Applied and Environmental Microbiology* **74**, 3985 (Jul, 2008).
21. M. A. de Angelis, M. D. Lilley, E. J. Olson, J. A. Baross, *Deep-Sea Research Part I-Oceanographic Research Papers* **40**, 1169 (1993).
22. G. R. Dickens, J. R. Oneil, D. K. Rea, R. M. Owen, *Paleoceanography* **10**, 965 (Dec, 1995).
23. M. E. Katz, D. K. Pak, G. R. Dickens, K. G. Miller, *Science* **286**, 1531 (1999).
24. D. F. McGinnis, J. Greinert, Y. Artemov, S. E. Beaubien, A. Wuest, *Journal of Geophysical Research-Oceans* **111**, (Sep 2, 2006).
25. G. Rehder, I. Leifer, P. G. Brewer, G. Friederich, E. T. Peltzer, *Marine Chemistry* **114**, 19 (Apr 20, 2009).
26. This research was supported by the National Science Foundation through grants OCE 1042650 and OCE 0849246 to JDK, OCE 1042097 and OCE 0961725 to DLV, and by the Department of Energy (DE-NT0005667) to DLV. The August, September, and October expeditions were funded by the National Oceanic and Atmospheric Administration through a contract with Consolidated Safety Services, Inc. We thank the Officers and crew of the NOAA Ship *Pisces*, as well as S. Joye, M. Heintz, C. Farwell, F. Kinnaman, K. Mouyard, T. Bryant, B. Pierce, A. Lee, R. Hansman, S. Socolofsky, L. Hu, F. Garcia Tigreros, T. Bianchi, X. Li, S. DiMarco, S. Bagby, G. Paradis, and the staff at Picarro Inc. and Los Gatos Research Inc. for valuable technical assistance and discussions. Sequences are available on GenBank, accession numbers HQ433363-HQ433432 and HQ652514-HQ652537.

Supporting Online Material

www.sciencemag.org/cgi/content/full/science.1199697/DC1
Materials and Methods
Figs. S1 to S6
Table S1
References

28 October 2010; accepted 20 December 2010
Published online 06 January 2011; 10.1126/science.1199697

Figure 1. (**A**) Sampling stations overlaid on a Google Earth image highlighting the area of the intrusion. Blue plus, red diamond, and white triangle symbols indicate sampling stations for the 18 August – 2 September, 7 – 17 September, and 22 September – 4 October 2010, expeditions respectively. The yellow and green boundaries indicate the extent of the contouring bounds as determined from the extent of the DO and fluorescence anomalies and bathymetric restrictions. (**B**) Contour plot within the yellow boundary of the vertically integrated DO anomaly at each station using data from the 18 August – 2 September 2010 expedition. Units are moles DO m^{-2}. (**C**) Profiles of DO (SBE-43, Sea-Bird Electronics Inc.; red line calibrated with Winkler titrations) and fluorescence (UV AquaTracka (Emission = 360nm), Cheslea Technologies Group; black line). The green circles represent Winkler titration samples. Station PC198 (26.7098ºN, 90.6286ºW).

Figure 2. Results from DNA surveys for bacterial 16S rRNA genes representing changes in community structure associated with oxidation of CH_4 in samples collected from 7-17 September 2010. Stations are shown from left to right in order of decreasing reductions in DO. Stations 192, 222, 230, and 211, had DO and fluorescence anomalies (integrated oxygen reductions of 1.1, 0.7, 0.5, and 0.1 mol/m^2, respectively), while stations 191, 242 and 203 did not (integrated oxygen reductions <0.00001 mol/m^2). Methylotrophs (*Methylococcaceae*, *Methylophaga*, and *Methylophilaceae*) are indicated by shading. The "Other" category includes groups observed at <5% in all samples, predominately *Acidobacteria, Actinobacteria*, and *Verrucomibrobia*. n = 56 – 79 per station for a total of 492.

Figure 3. Model results from a one-dimensional time-dependent model of (●) average DO anomaly from CH_4 respiration (μM reduction in the intrusion layer), (□) average CH_4 concentration (μM), and (×) first-order CH_4 oxidation rate constants ($days^{-1}$) in the intrusion layers. Labels (**A**) – (**D**) on the figure represent measured values. (**A**) Avg CH_4 Concentration = 25 μM (range = 0.57 – 183 μM; n = 73), 11-20 June (*11*); (**B**) Avg CH_4 concentration = 1.43 ± 2.00 nM (n = 671), Avg CH_4 oxidation rate constant = 0.0015 $days^{-1}$ (range = 0.0005 – 0.0038 day^{-1}, n = 10), 7-17 September; (**C**) Avg CH_4 oxidation rate constant = 0.001 day^{-1} (range = 0 – 0.0127 day^{-1}, n = 22 minus one outlier), 11-20 June (*11*); (D_M) Max Dissolved O_2 Anomaly = 36.7 μM, (D_A) Avg Dissolved O_2 Anomaly = 5.6 ± 5.8 μM (n = 202), 18 August – 4 October, 2010.

Table 1. Hydrocarbon emission estimates and oxygen removal potentials (*13*).

Hydrocarbon	Quantity Emitted (moles)	Stoichiometric Ratio O_2:Hydrocarbon	O_2 Removing Potential (moles)	Dissolved O_2 Removed (moles)
CH_4	$0.91 – 1.25\times10^{10}$	2:1	$1.83 – 2.50\times10^{10}$	
C_2H_6	$0.85 – 1.16\times10^{9}$	3.5:1	$2.96 – 4.05\times10^{9}$	
C_3H_8	$4.60 – 6.28\times10^{8}$	5:1	$2.30 – 3.14\times10^{9}$	
Oil[a] as $(-CH_2-)$	$0.93 – 1.00\times10^{10}$	1.5:1	$1.40 – 1.50\times10^{10}$	
		Total	$3.76 – 4.72\times10^{10}$	$3.00 – 3.90\times10^{10}$

[a] = only oil in the deepwater intrusion layers

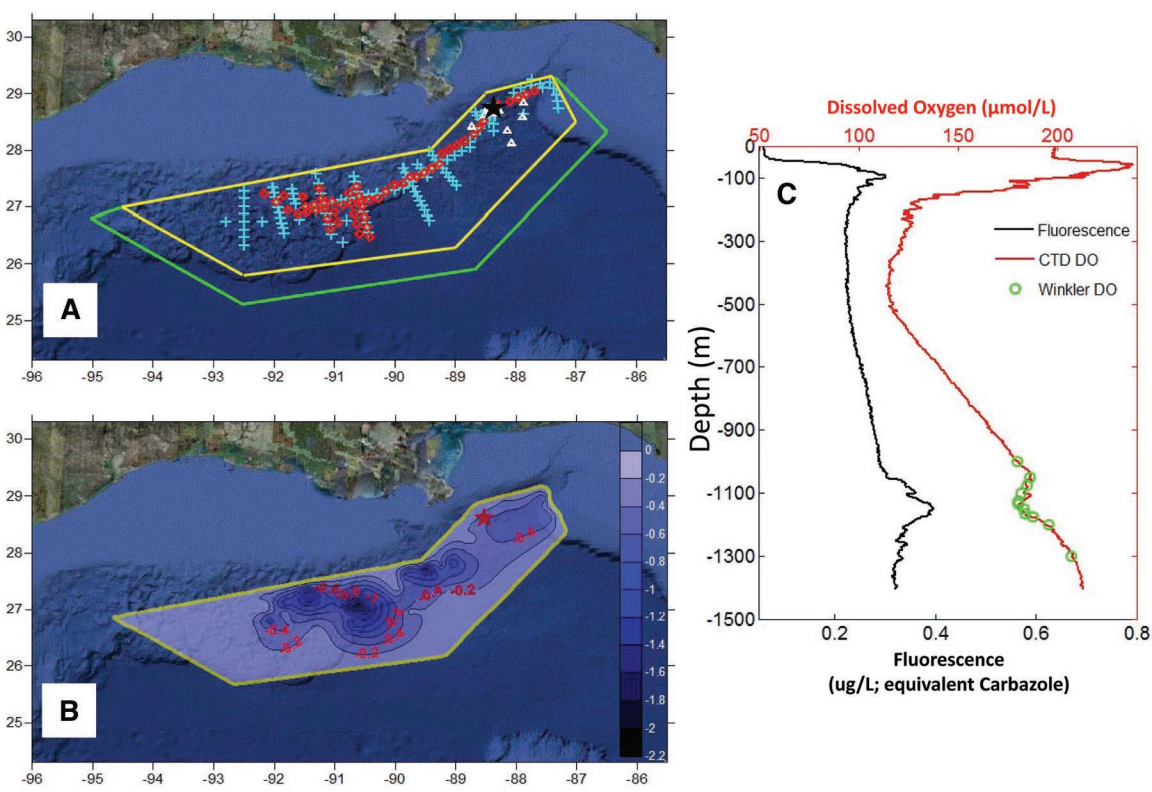
A
B
C
Dissolved Oxygen (µmol/L)
50
100
150
200
Fluorescence
CTD DO
Winkler DO
Depth (m)
0
-100
-300
-500
-700
-900
-1100
-1300
-1500
0.2
0.4
0.6
0.8
Fluorescence
(ug/L; equivalent Carbazole)
30
29
28
27
26
25
-96
-95
-94
-93
-92
-91
-90
-89
-88
-87
-86

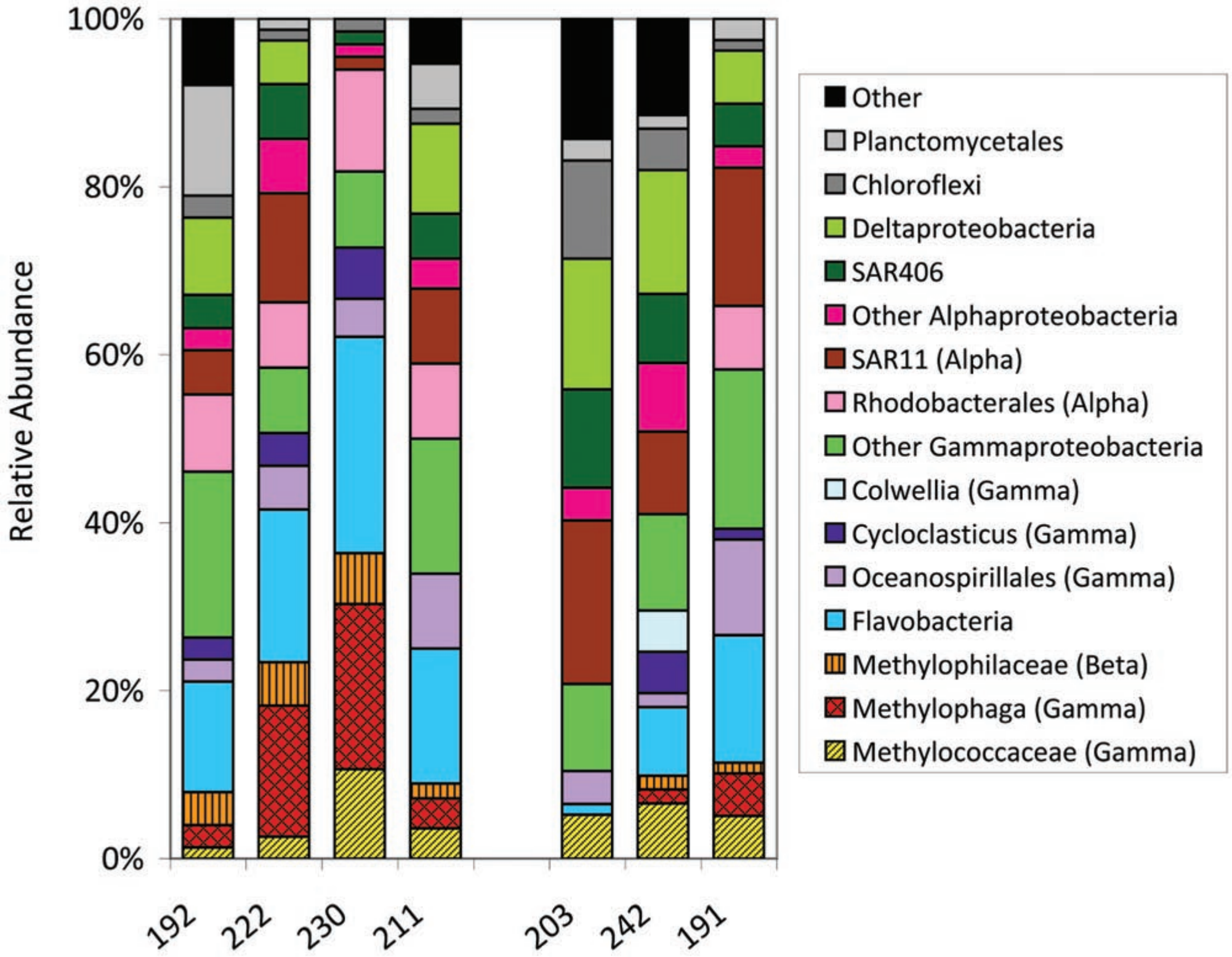
100%
80%
60%
40%
20%
0%
Relative Abundance
192
222
230
211
203
242
191
Other
Planctomycetales
Chloroflexi
Deltaproteobacteria
SAR406
Other Alphaproteobacteria
SAR11 (Alpha)
Rhodobacterales (Alpha)
Other Gammaproteobacteria
Colwellia (Gamma)
Cycloclasticus (Gamma)
Oceanospirillales (Gamma)
Flavobacteria
Methylophilaceae (Beta)
Methylophaga (Gamma)
Methylococcaceae (Gamma)

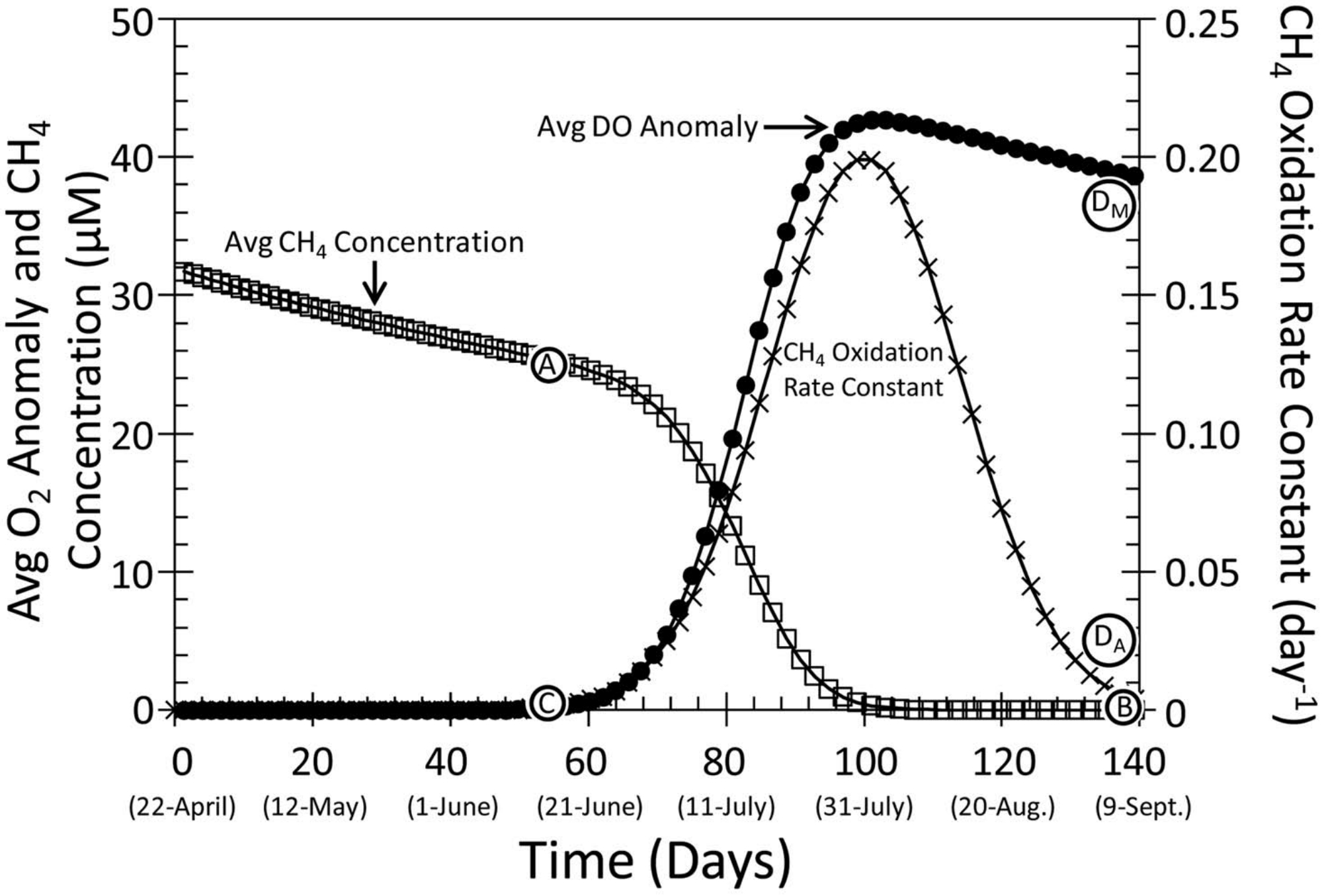
Avg O_2 Anomaly and CH_4 Concentration (μM)
CH_4 Oxidation Rate Constant (day^{-1})
Time (Days)
Avg DO Anomaly
Avg CH_4 Concentration
CH_4 Oxidation Rate Constant
A
B
C
D_M
D_A
50
40
30
20
10
0
0.25
0.20
0.15
0.10
0.05
0
0 (22-April)
20 (12-May)
40 (1-June)
60 (21-June)
80 (11-July)
100 (31-July)
120 (20-Aug.)
140 (9-Sept.)

Supporting Online Material for

A Persistent Oxygen Anomaly Reveals the Fate of Spilled Methane in the Deep Gulf of Mexico

John D. Kessler,* David L. Valentine,* Molly C. Redmond, Mengran Du, Eric W. Chan, Stephanie D. Mendes, Erik W. Quiroz, Christie J. Villanueva, Stephani S. Shusta, Lindsay M. Werra, Shari A. Yvon-Lewis, Thomas C. Weber

*To whom correspondence should be addressed. E-mail: jkessler@ocean.tamu.edu (J.D.K.); valentine@geol.ucsb.edu (D.L.V.)

Published 6 January 2011 on *Science* Express
DOI: 10.1126/science.1199697

This PDF file includes:

Supporting Online Material for

Title: A persistent oxygen anomaly reveals the fate of spilled methane in the deep Gulf of Mexico

Authors:

John D. Kessler[1*], David L. Valentine[2*], Molly C. Redmond[2], Mengran Du[1], Eric W. Chan[1], Stephanie D. Mendes[2], Erik W. Quiroz[3], Christie J. Villanueva[2], Stephani S. Shusta[2], Lindsay M. Werra[2], Shari A. Yvon-Lewis[1], Thomas C. Weber[4]

[1]Department of Oceanography, Texas A&M University, College Station, TX 77843-3146; [2]Department of Earth Science and Marine Science Institute, University of California, Santa Barbara, CA 93106; [3]Geochemical and Environmental Research Group, Texas A&M University, College Station, TX 77843; [4]Center for Coastal and Ocean Mapping, University of New Hampshire, Durham, NH 03824

[*]Kessler and Valentine contributed equally to this work; thus, correspondence should be addressed to both authors: jkessler@ocean.tamu.edu, valentine@geol.ucsb.edu

Hydrocarbon emission estimates and potential impacts on dissolved oxygen. The molar quantity of oil and gas emitted during the Deepwater Horizon spill was calculated using similar procedures as was presented in Valentine *et al.* (*S1*); however, the estimates were updated given recent estimates of the gas to oil ratio and the total oil released. The gas to oil ratio was updated from what was used previously (*S1*) to 2200 cubic feet of gas (14.73 psia, 60°F) per barrel of oil based on data released from the US

Department of Energy (*S2*). However, because it is unknown if gas fractionation occurred during the containment efforts, a range of values are used (2200 to 2800 cubic feet of gas per barrel of oil). The total oil emission presented in Valentine *et al.* (*S1*) was 4,101,054 bbl which was from the USGS/NOAA oil balance report released in preliminary form on Aug 1, 2010 (*S3*). A second report (*S4*) used optical intrusion velocimetry to estimate that $4.4 \times 10^6 \pm 20\%$ bbl of oil were released, which encompasses the estimate from the USGS/NOAA oil balance report. Nonetheless, we assume a range of oil emitted spanning the two reports 4.1 to 4.4×10^6 bbl (Table 1). The USGS/NOAA oil balance report estimates that 23.6% of the emitted oil is retained within the intrusion layers based on estimates of natural and chemical dispersion (*S3*). This intrusion layer oil percentage is applied to both oil emission estimates.

One-Dimensional Time-Dependent Box Model of Methane Oxidation Rates: In order to test various scenarios for the fate of the dissolved CH_4 intrusion and its impact on dissolved O_2, we assembled a model of diffusion, advective mixing, and CH_4 oxidation. Diffusion was modeled using a similar approach (one-dimensional box model) as was presented previously (*S5- S9*) and determined to be insufficiently slow to account for any noticeable decrease in the CH_4 intrusion (Eq. S1).

$$\frac{dn_i}{dt} = K_i \frac{(C_{i-1} - C_i)}{\Delta z} A_i + K_{i+1} \frac{(C_{i+1} - C_i)}{\Delta z} A_{i+1} \qquad \text{(Eq. S1)}$$

Here, dn_i/dt is the time rate of change of the number of moles of CH_4 in box i, A_i and A_{i+1} are the areas of the top and bottom of the boxes, K_i and K_{i+1} are the eddy diffusion coefficients at the top and bottom of the boxes (area per time), C_i is the CH_4 concentration in the box, and C_{i-1} and C_{i+1} are the CH_4 concentration for the boxes $i-1$ and $i+1$. Even with the diffusion constant set unreasonably high at 10 cm^2 s^{-1}, the maximum concentration in the intrusion decreases by only 4% in 50 years; thus diffusion was deemed insignificant and removed from model consideration.

A simple advective mixing model was assembled in one-dimension (Eq. S2).

$$\frac{dC}{dt} = V \times \frac{\partial C}{\partial X} \qquad \text{(Eq. S2)}$$

Here, dC/dt is the time rate of change of the CH_4 concentration in the box, $\partial C/\partial X$ is the distance rate of change of CH_4 concentration in one dimension, and V is the current velocity. The model assumes that the CH_4 concentration is distributed with distance following a normal Gaussian. The advective velocity was varied to generously bound the observed velocities measured via Acoustic Doppler Current Profiler (ADCP) on the Deepwater Horizon and relief well rigs, while the average velocity at 1000 m depth during this time period approximately equaled 3 km day^{-1} (*S10*). The normally distributed CH_4 concentration intrusion was divided into 50 equally spaced lateral boxes. As CH_4 from one box is advected into the adjacent box (at a rate determined by the ADCP data), the parcels of water are allowed to mix evenly before the newly mixed parcel advects into the adjacent box. This mixing is likely too aggressive as adjacent parcels can move in unison minimizing mixing; nonetheless, this simulation provides an upper boundary for the dilution of the CH_4 intrusion due to advective mixing. In addition to advective mixing, we incorporated a term for first-order CH_4 oxidation rates. An intrusion thickness of 200 m and width of 25 km were assigned to match what was measured here and has been reported previously (*S1, S11*). The amplitude of the CH_4 concentrations in the intrusion and standard deviation of the concentration distribution with intrusion length were varied to match average observed values (25 μM; range = 0.57 – 183 μM; n = 73) in a previous June expedition (*S1*) as well as average values of dissolved O_2 (DO) anomalies measured during the three expeditions documented here (5.6 ± 5.8 μM (n = 202) reduction in DO in the intrusion layer). Methane oxidation rate constants were varied with time following a Gaussian distribution to simulate a bloom and bust cycle of methanotrophs. Average measured methane oxidation rates were low during June (0.001 day^{-1}; range = 0 – 0.0127 day^{-1}; n = 22 minus one outlier) (*S1*) and September (0.0015 day^{-1}; range = 0.0005 – 0.0038 day^{-1}; n = 10) and were used to set the bounds for the time-dependent distribution of methane oxidation rates. The amplitude and standard deviation of this time-dependent oxidation rate constant distribution were varied along with the spatially variable starting

CH_4 concentration distribution to match observed values of CH_4 concentration, DO anomalies, and CH_4 oxidation rates (Figs. 3 and S1).

Dissolved Oxygen Analysis: Dissolved oxygen (DO) was continuously recorded by the electrode-based oxygen sensor (SBE-43) on the *Pisces'* CTD rosette and was measured at select depths by the Winkler procedure; these procedures have been previously published (*S1*). Repeated analysis of the standard sodium thiosulfate with an amperometric oxygen titration system used during the September and October expeditions gave a value of 0.70469 ± 0.00121 μL and blank of 0.00316 ± 0.00059 μL (mean ± stdev; n = 24). The continuous SBE-43 profiles were corrected for drift with linear least squares equation derived from the SBE-43 data and Winkler titration data at each station.

The results from the Winkler titration showed good agreement with the SBE-43. A 10th order polynomial was fit to Winkler-calibrated SBE-43 data to obtain the background dissolved oxygen profile at each station. The oxygen anomaly was derived by subtracting the Winkler-derived oxygen concentration from the corresponding background value (Fig. S2); this most likely provides a conservative estimate of the oxygen anomaly because reductions in DO that have been diluted vertically will be difficult to distinguish from background. Contour maps were drawn by Golden Software Surfer with the Kriging, minimum curvature, natural neighbor, radial basis function, and triangulation with linear interpolation gridding methods (95°W – 86.5°W, 25.3°N – 29.3°N, 100×58 grids) in order to estimate the influence of the contour algorithm on the estimate of total moles of DO removed from the intrusion layer (Fig. S3; Table S1). Values for the contour maps were extracted at equally spaced grid intervals (8305 m east to west, 7839 m north to south) over the contouring area and used to determine the total moles of DO removed (Fig. S3). Two areas were selected to calculate the total oxygen depletion

(Figs. 1A and S3). Bounds for the contouring on the northern and eastern edges were chosen based on bathymetric restrictions. On the southern and western edges, bounds were defined to encompass the DO and fluorescence anomalies measured with an average buffer of 50 km to incorporate any anomalies that may have been missed during sampling (Figs. 1A and S3, Yellow Boundary). The area bounded in green is simply an extension of the yellow area by 50 km on the southern and western edges in order to estimate the influence of the bounding area on the total loss of DO (Figs. 1A and S3, Green Boundary). The northern and eastern edges were not extended in a similar fashion as that would encompass shallow bathymetry that does not contain the intrusion CH_4. We assume that no oxygen is depleted outside the selected area and depletions along boundaries are set to zero prior to contouring (Tables 1 and S1).

The total amount of DO removed from the intrusion layer was greatest during the August expedition and decreased during the September-October expeditions. Two or more explanations are possible. (1) The largest DO anomalies simply were not sampled during the September – October expeditions, thereby biasing the contouring toward lower values. (2) The integration method for vertical anomalies was overly conservative in defining the baseline condition (as described above), and thereby was more biased against the more diluted (but covering larger aerial extent) anomalies present in September and October. Whichever explanation is true is irrelevant, since a near quantitative removal of the intruded methane appears to have occurred by the August expedition. Thus, we use the DO deficit recorded during the August expedition as a proxy for the maximum amount of DO which was removed from the intrusion layer during this disaster (Tables 1 and S1).

Quantification of methane, ethane, and propane concentrations. Samples for methane, ethane, and propane concentrations were collected and prepared as described previously (*S1*). Samples were stored in a cold room at 4°C for 12 hours. The temperature of the samples was recorded before analysis.

Concentrations were measured by gas chromatography (GC), using a Shimadzu GC-14A equipped with a flame ionization detector (FID).

Quantification of methane oxidation rates. Samples were collected and treated in a similar manner described previously for ethane and propane oxidation rates (*S1*). Modifications include using 99% ^{13}C-methane, instead of ethane and propane, as the tracer. The dissolved inorganic carbon (DIC) of the samples was analyzed in an identical method as described previously (*S1*), using isotope ratio mass spectrometry to measure differences in DIC between enriched and background samples.

16S rRNA Libraries and Phylogenetic Trees: 1 L seawater samples from seven sites were filtered onto 0.2 μm Sterivex filters (Millipore) and stored frozen. DNA was extracted from filters with the FastDNA spin kit for soil (MP Biomedicals). The 16S rRNA gene was amplified with the primers 27F and 1392R, as previously described (*S12*). Duplicate 50 μl PCR reactions were pooled and cleaned with the Wizard SV DNA purification kit (Promega) and cloned with the PCR cloning kit (Qiagen). Clones were selected at random and purified plasmid DNA (Mo Bio UltraClean Mini Plasmid Prep Kit) was sequenced at the UC Berkeley DNA Sequencing Facility. Sequences were edited and assembled with Sequencher (Gene Codes Corporation), and potential chimeras were detected using Bellerophon (*S13*) and Pintail (*S14*). Suspected chimeras and low quality sequences were eliminated from analysis, leaving 56-79 sequences per site (492 total). Sequences were assigned to taxonomic groups using the RDP Classifier tool (*S15).* Most sequences were assigned to family level taxa, with the exception of Methylophaga and Cycloclasticus, which were assigned at the genus level. To show the depth of coverage in the clone libraries, rarefaction curves (Fig. S4) were computed using EstimateS (Version 8.2, R. K. Colwell, http://purl.oclc.org/estimates), with OTUs grouped at the family level. Representative members of each taxa were aligned with CLUSTALW, and MEGA4 (*S16*) was used to construct neighbor-joining

phylogenetic trees, using the maximum composite likelihood method and 2000 bootstrap replicates. The number of sequences included in trees was limited for clarity, but all unique sequences (<98% similar) were submitted to Genbank under the accession numbers HQ433363-HQ433432 and HQ652514-HQ652537 (Figs. 2 and S5). The particulate methane monooxygenase gene was amplified in three plume samples (192, 222, and 230) with the standard pmoA primers A189f and mb661r (S18), as well as modified versions of these primers, wcpmoA189f and wcpmoA661r (S19). Amplification was very poor with the first set of primers, but excellent with the second, designed to optimize amplification for marine water column methanotrophs. Only PCR product from the modified primers was used for cloning, as described above. Phylogenetic analysis of the inferred amino acid sequences was conducted with MEGA, also as described above.

References

S1. D. L. Valentine *et al.*, *Science* **330**, 208 (2010).

S2. Department of Energy. Deepwater Horizon Response. http://www.energy.gov/open/oilspilldata.htm

S3. USGS, "Deepwater Horizon MC252 gulf Incident Oil Budget: Government Estimates - Through August 01 (Day 104)" (2010). Available at: http://www.noaanews.noaa.gov/stories2010/PDFs/DeepwaterHorizonOilBudget20100801.pdf

S4. T. J. Crone, M. Tolstoy, *Science* (2010) (10.1126/science.1195840).

S5. M. I. Scranton, *Deep-Sea Research* **35**, 1511 (1988).

S6. M. I. Scranton, F. L. Sayles, M. P. Bacon, P. G. Brewer, *Deep-Sea Research* **34**, 945 (1987).

S7. J. D. Kessler *et al.*, *Earth and Planetary Science Letters* **243**, 366 (2006).

S8. J. D. Kessler, W. S. Reeburgh, J. Southon, R. Varela, *Geophysical Research Letters* **32**, (2005).

S9. J. D. Kessler, W. S. Reeburgh, S. C. Tyler, *Global Biogeochemical Cycles* **20**, (2006).

S10. National Data Buoy Center. National Oceanic and Atmospheric Administration. http:///ndbc.noaa.gov/

S11. R. Camilli *et al.*, *Science* **330**, 201 (2010).

S12. M. C. Redmond, D. Valentine, A. L. Sessions, *Appl. Environ. Microbiol.* **76**, 6412 (2010).

S13. T. Huber, G. Faulkner, P. Hugenholtz, *Bioinformatics* **20**, 2317 (2004).

S14. K. Ashelford, N. Chuzhanova, J. Fry, A. Jones, A. Weightman, *Appl. Environ. Microbiol.* **71**, 7724 (2005).

S15. Q. Wang, G. Garrity, J. Tiedje, J. Cole, *Appl. Environ. Microbiol.* **73**, 5261 (2007).

S16. K. Tamura, J. Dudley, M. Nei, S. Kumar, *Mol. Biol. Evol.* **24**, 1596 (2007).

S17. T. C. Hazen *et al.*, *Science* **330**, 204 (2010).

S18. Costello AM, ME Lidstrom, *Appl. Environ. Microbiol.* **65,** 5066-5074 (1999).

S19. Tavormina P, Ussler III W, Orphan, **74**, 3985-3995 (2008).

Table S1. Total amount of dissolved O_2 removed ($\times 10^{10}$ moles)

	Yellow Area			Green Area		
Contouring Method	Expedition 1	Expedition 2	Expeditions 2 + 3	Expedition 1	Expedition 2	Expeditions 2 + 3
Kriging	3.29	2.25	2.13	3.90	3.08	2.84
Minimum Curvature	3.10	1.83	1.72	3.52	2.73	2.49
Natural Neighbor	3.02	1.99	1.89	3.61	2.69	2.46
Radial Basis Function	3.19	2.30	2.17	3.81	3.24	2.97
Triangulation	3.00	1.95	1.84	3.59	2.67	2.36

Expedition 1 = 18 August – 2 September 2010
Expedition 2 = 7 September – 17 September 2010
Expedition 3 = 22 September – 4 October 2010

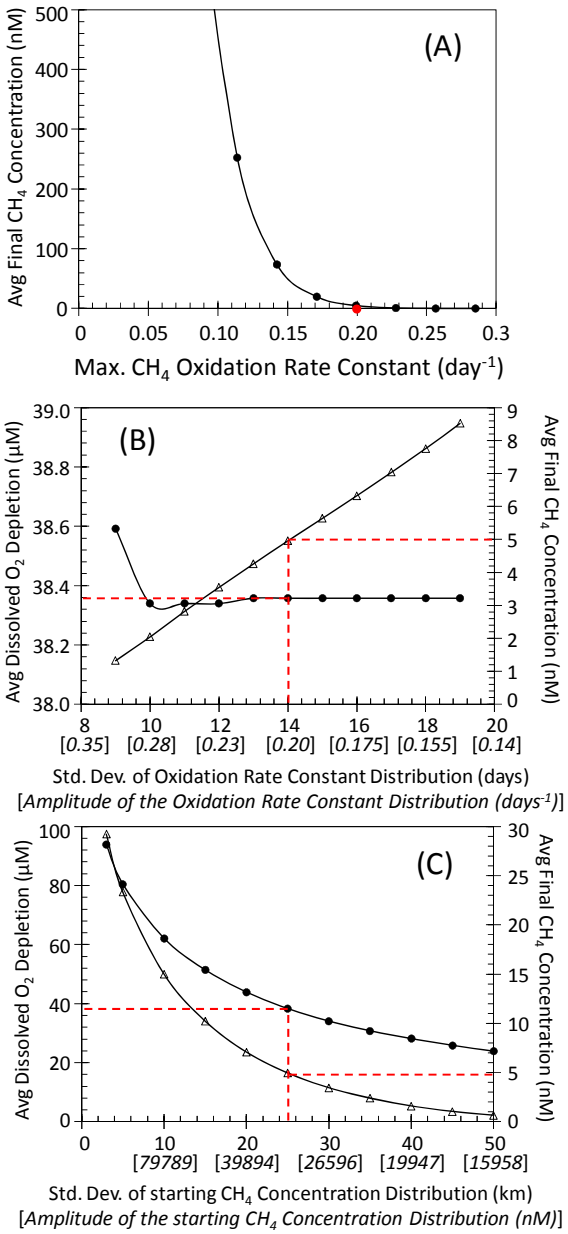

Figure S1. (A) The influence of increasing the maximum CH_4 oxidation rate constant on the final (mid-September) average CH_4 concentration while keeping the standard deviation of the distribution of oxidation rates constant at 14 days. The red dot signifies the minimum oxidation rate constant necessary to achieve the CH_4 concentrations measured in the August-October expeditions. **(B)** Standard deviation of oxidation rate constant distribution (days) vs. (●) average DO anomaly in the intrusion (µM reduction) and (Δ) average final CH_4 concentration (nM). The dotted red lines indicate the standard deviation of the oxidation rate constant distribution necessary to model the measured DO anomaly and average final CH_4 concentration. **(C)** Standard deviation of the starting CH_4 concentration distribution (km) vs. (●) average DO anomaly (µM reduction) and (Δ) average final CH_4 concentration (nM). The dotted red lines indicate the standard deviation of the starting CH_4 concentration distribution necessary to model the measured DO anomaly and average final CH_4 concentration.

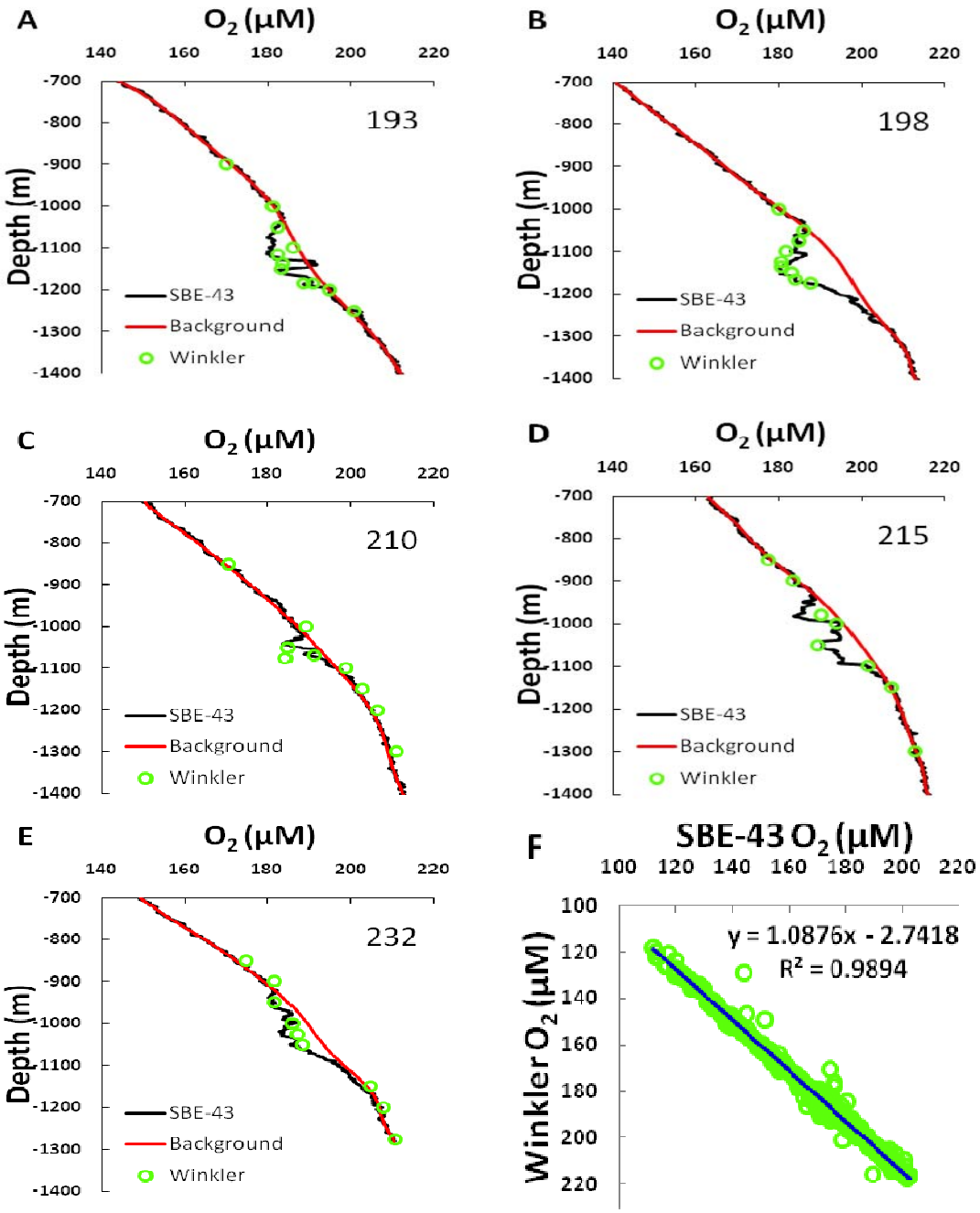

Figure S2. Dissolved O_2 measured with the (black line) electrode-based O_2 sensor (SBE-43) and (green circles) Winkler titrations. A background was fit to the data using a 10th order polynomial (red line) and was used to calculate the DO anomalies. The Winkler titrations both calibrated the SBE-43 readings and confirmed the presence of DO anomalies in the intrusion layer. Station numbers are indicated in the upper-right corner of the figures. A plot of SBE-43 vs. Winkler data yields a linear relationship again validating the DO anomalies recorded in the intrusion layer.

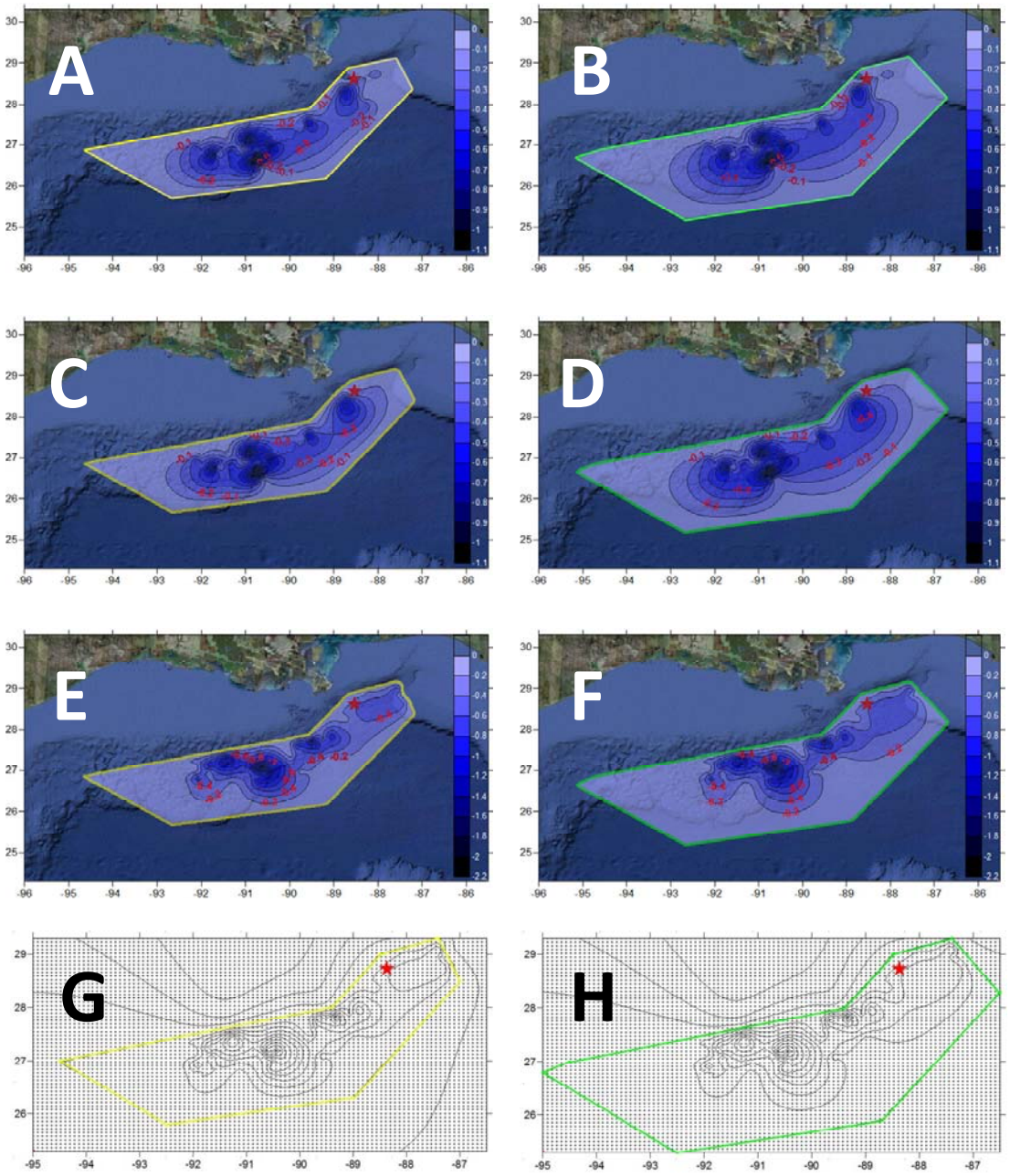

Figure S3. Contour plots of the vertically integrated DO anomaly (in units of moles DO m^{-2}) at each station overlaid on a Google Earth image. The star indicates the wellhead. (A) Yellow boundary, 7 – 17 September + 22 September – 4 October 2010 expeditions. (B) Green boundary, 7 – 17 September + 22 September – 4 October 2010 expeditions. (C) Yellow boundary, 7 – 17 September 2010 expedition. (D) Green boundary, 7 – 17 September 2010 expedition. (E) Yellow boundary, 18 August – 2 September 2010 expedition. (F) Green boundary, 18 August – 2 September 2010 expedition. (G) Gridding used to extract the contour values. Yellow boundary, 18 August – 2 September 2010 expedition. (H) Gridding used to extract the contour values. Green boundary, 18 August – 2 September 2010 expedition.

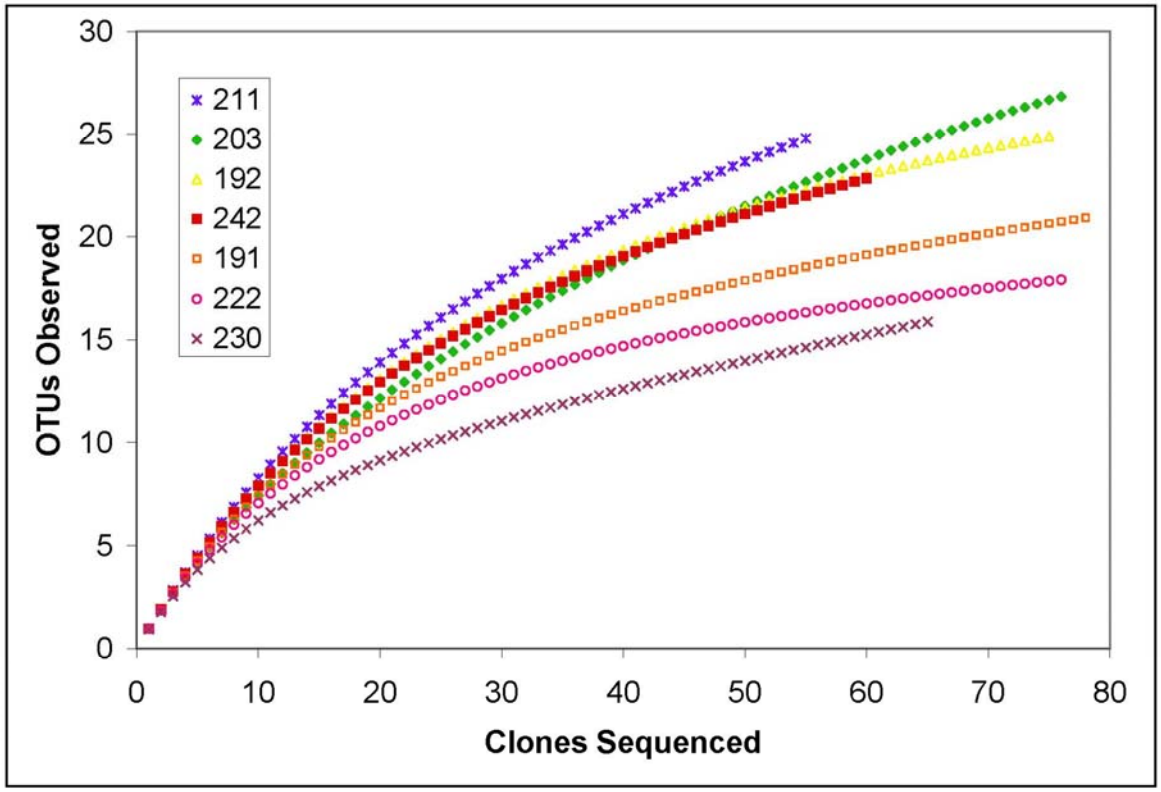

Figure S4. Rarefaction curves showing the relationship between the number of operational taxonomic units (OTUs) observed and the number of clones sequenced. OTUs were determined with the RDP Classifier Tool (*S15*) at the family level. DNA yield in ng l^{-1} (by station) is as follows: 145 (211); 232 (203); 170 (192); 213 (242); 114 (191); 208 (222); 113 (230).

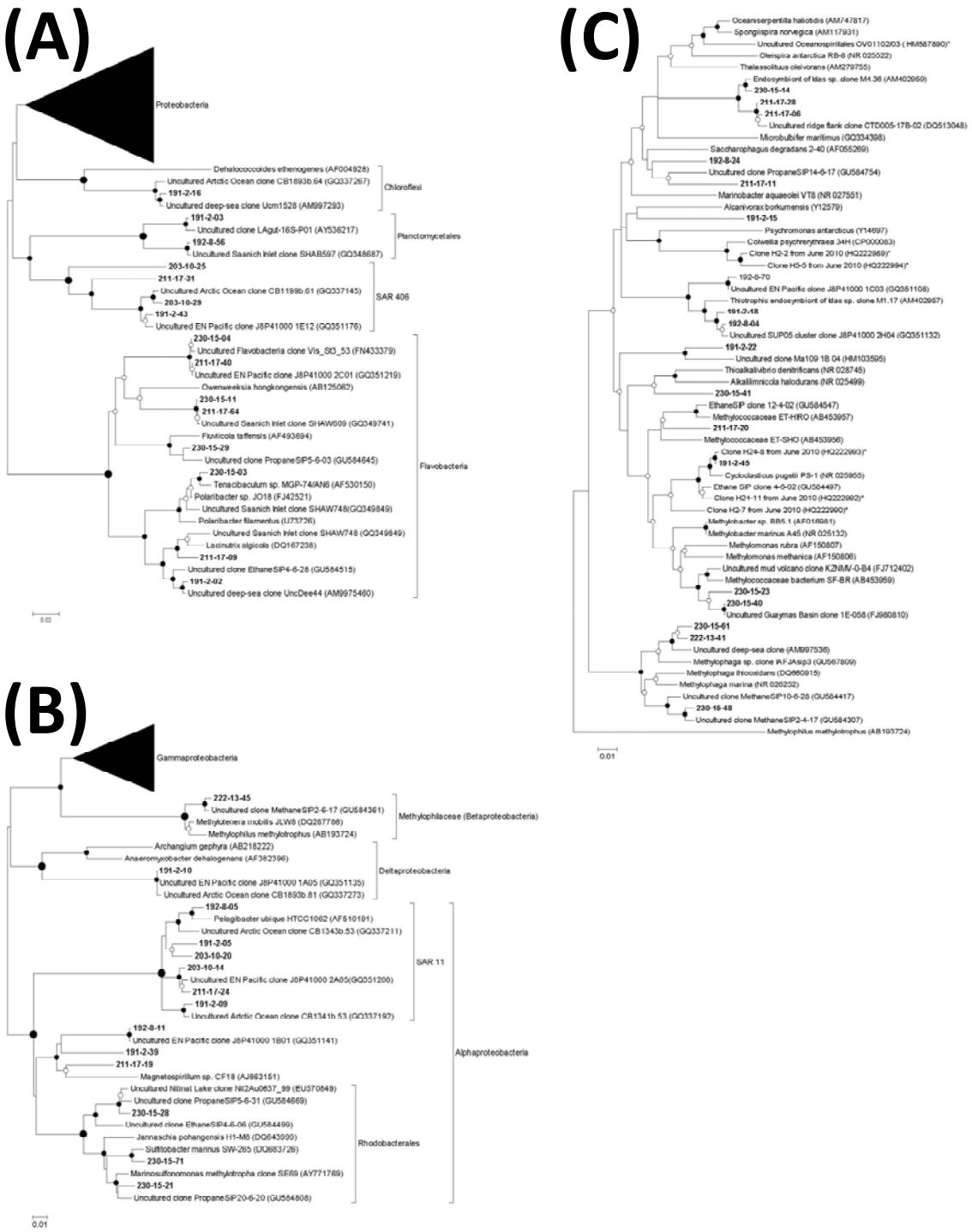

Figure S5. Neighbor-joining phylogenetic trees, showing (A) all major bacterial groups in these samples, (B) the *Proteobacteria*, and (C) the *Gammaproteobacteria*. Sequences from this study are in bold, while sequences observed in May and June by Valentine *et al.* (*S1*) and Hazen *et al.* (*S17*) are marked with *. Filled circles indicate bootstrap values above 90% and open circles indicate bootstrap values above 50% (1000 bootstrap replicates).

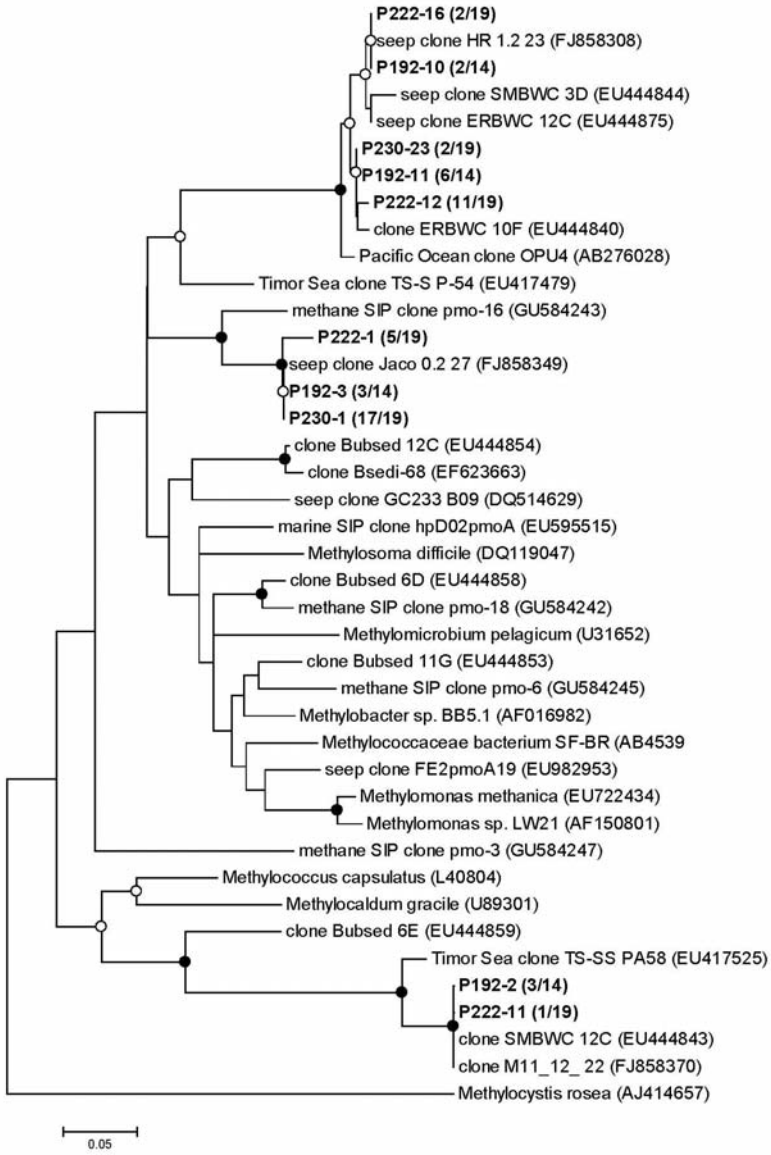

Figure S6. Neighbor-joining phylogenetic tree of inferred amino acid seqeunces encoded by the pmoA gene. Sequences from this study (sites 192, 222, and 230) are shown in bold and the number of clones represented by each sequence is shown in parentheses, as a fraction of total clones from that sample; reference sequences from GenBank are also included (accession numbers in parentheses. Filled circles indicate bootstrap values above 90% and open circles bootstrap values above 50% (2000 replicates).